TRANSPORT AND LOSSES OF FUSION-BORN ALPHA PARTICLES IN THE PRESENCE OF MHD INSTABILITIES A passive tracer approach using the new full-orbit Toroidal Accelerated PArticle Simulator (TAPAS)

David Zarzoso, Homam Betar, Diego Del-Castillo-Negrete, Jacobo Varela, Luis Garcia, Jeronimo Garcia, Yevgen Kazakov

TRANSPORT AND LOSSES OF FUSION-BORN ALPHA PARTICLES IN THE PRESENCE OF MHD INSTABILITIES

*A passive tracer approach using the new full-orbit Toroidal Accelerated PArticle Simulator (*TAPAS*)*

[1]D. ZARZOSO, [1]H. BETAR, [2]D. DEL-CASTILLO-NEGRETE, [3]J. VARELA, [3]L. GARCIA, [2]D. SPONG, [4]J. GARCIA, [5]Y. KAZAKOV and JET CONTRIBUTORS*

[1] Aix-Marseille University, CNRS, Centrale Marseille, M2P2 UMR 7340, Marseille, France
[2] Oak Ridge National Laboratory, Oak Ridge, TN 37831-8071, United States of America
[3] Universidad Carlos III de Madrid, 28911 Leganes, Madrid, Spain
[4] CEA, IRFM, F-13108 Saint-Paul-lez-Durance, France.
[5] Laboratory for Plasma Physics, LPP-ERM/ KMS, TEC Partner, Brussels, Belgium
*See the author list of "Overview of T and D-T results in JET with ITER-like wall" by CF Maggi et al. to be published in Nuclear Fusion Special Issue: Overview and Summary Papers from the 29th Fusion Energy Conference (London, UK, 16-21 October 2023)
Email: david.zarzoso-fernandez@univ-amu.fr

Abstract

The confinement of highly energetic alpha particles is of uttermost importance, for they must transfer their energy to the thermal plasma in order to ensure the self-sustainment of fusion reactions. The present paper focuses on this issue by combining gyro-fluid modelling of a recent JET discharge using the FAR3d code and the integration of trajectories of passive fusion-born alpha particles using the recently developed full-orbit Toroidal Accelerated PArticle Simulator (TAPAS). Special emphasis is put on the impact of magnetohydrodynamic activity triggered by energetic particles on the confinement of alpha particles. In the analysed discharge, significant population of trapped Hydrogen from Ion Cyclotron Resonant Heating drives fishbone unstable, which is observed in self-consistent simulations of FAR3d. The obtained electromagnetic perturbation is afterwards introduced in TAPAS to integrate the trajectories of alpha particles in the inner core. It is concluded that there is significant global impact of the fishbone instability on the losses of alpha particles. Preliminary analyses have also been conducted to assess the impact of other instabilities, such as those excited by the passing population resulting in Toroidicity-induced Alfvén Eigenmodes, with frequencies larger than that of the fishbone. The results show that the effect of these modes on the confinement of alpha particles might be negligible.

1. INTRODUCTION

Energetic particles are ubiquitous in present fusion plasmas, in particular energetic ions, which are born from the external heating, either Neutral Beam Injection (NBI) or Ion Cyclotron Resonant heating (ICRH). These ions exhibit energies much larger than the thermal velocity of the particles of the bulk plasma. Their presence ensures the heating of the thermal plasma by means of Coulomb collisions as well as the parallel current that can improve the confinement [1, 2]. It is nonetheless expected that the main heating in future fusion reactors comes from the thermalization of energetic (3.5 MeV) alpha particles generated by the fusion reactions between Deuterium and Tritium. These fusion-born alpha particles will transfer their energy first to the electrons, and afterwards (when their energy is below the critical energy) to the ion population. However, the presence of highly energetic ions in the plasma (either accelerated by external heating or generated by fusion reactions) can trigger instabilities which can result in significant transport and eventual losses of energetic ions, reducing this way the performance of present and future tokamaks. Of special importance is the impact of these instabilities on the confinement of fusion-born alpha particles, since degradation of their confinement can be deleterious to the achievement of steady-state regimes of energy production. For this reason, it is essential to understand and quantify the transport and losses of fusion-born alpha particles in the presence of MHD instabilities. In this context, the second D-T campaign (DTE2) that took place at the JET tokamak has represented a unique opportunity to conduct in-depth analyses of alpha particle physics in D-T plasmas. In the paper, we perform analyses of the losses of fusion-born alpha particles by modelling the JET discharge 99896 [3]. In this discharge, Deuterium and Tritium NBI heating was applied one after the other and combined with ICRH. The destabilization of fishbones at $f \sim 40$ kHz and Toroidicity-induced Alfvén Eigenmodes (TAEs) at $f \sim 150-190$ kHz was observed. To study the impact on alpha particle confinement, we proceed in two steps. First, we conduct numerical modelling of the discharge 99896 by

means of gyro-fluid simulations using FAR3d code [4]. The electromagnetic potential is then used to integrate trajectories of alpha particles using the full-orbit Toroidal Accelerated PArticle Simulator (TAPAS), updated from the original guiding-centre version [5]. It is to be noted that in the considered JET discharge, alpha particles do not drive any instability. Therefore, considering these particles as passive tracers in TAPAS is justified. The paper is structured as follows. Section 2 is devoted to describing the gyro-fluid modelling of the the JET discharge. In section 3 we provide an overview of the new TAPAS code. In section 4 we show the outcome of the analyses from the coupling FAR3d-TAPAS. Finally, in section 5 we summarize the results and give some future directions.

2. SUMMARY OF GYRO-FLUID MODELLING USING FAR3D CODE

The FAR3d code [4] evolves a set of reduced MHD equations for the thermal plasma, including Ohm's law, the parallel component of vorticity, pressure, and parallel velocity. Additionally, it includes two equations for each population of energetic particles: one for density and another for the parallel component of the energetic particle velocity. These latter equations are derived from the gyrokinetic equations and employ a two-pole Landau closure to close the system. Two scenarios have been modelled, highlighting the impact of trapped and passing population, owing to the presence of both NBI Deuterium and minority H for ICRH in the plasma. The first nonlinear simulation focuses on a regime composed of trapped Hydrogen and alpha particles, while the second simulation investigates the dynamics of passing Hydrogen. For the two simulations, we set the magnetic field at the magnetic axis to $B_0 = 2.96$ T, the major radius is $R_0 = 2.845$ m, the minor radius is $a = 1.14$, the temperature of the energetic particles at the magnetic axis is set to $T_{\rm EP} = 1000$ keV, and the the Lundquist number is $S = 10^7$. Furthermore, finite Larmor radius effects are considered for both thermal ions and energetic particles. The magnetic equilibrium used for these analyses has been computed using the VMEC code applied to the JET discharge 99896.

In the first simulation involving trapped hydrogen and alpha particles, we set $\beta_{\rm EP} = 0.4$ and $\beta_\alpha = 0.001$ for trapped hydrogen and alpha particles, respectively. This large β value of trapped energetic hydrogen primarily results from the temperature of the particles rather than their density ($n_{\rm EP} = 0.007 \times 10^{-20} m^{-3}$), which is 60 times smaller than that of the thermal plasma. The dominant modes in this simulation have been identified as fishbones excited by the trapped population, characterized by toroidal mode number $n = 1$ family and rather low frequencies ($f \sim 40$ kHz). Additionally, during the nonlinear phase, modes such as $1/1$, $2/2$, $3/3$, and $4/4$ contributed to the overall dynamics. The electromagnetic perturbation resulting from this first simulation is observed to be located at the inner region of the tokamak, as can be seen in the first two panels of Fig. 1, which shows the poloidal cross sections of the magnetic (first panel) and electrostatic (second panel) potentials at the saturated phase. A clear $m = 1$ structure is evidenced.

In the second simulation, which focused on studying the dynamics in the presence of passing population, we set $\beta_{EPs} = 0.3$. In this case, the dominant Toroidicity-induced Alfvé Eigenmodes (TAEs) corresponding to the $n = 3$ family were observed during the linear and saturation phases of the simulation. The electromagnetic perturbation during the linear phase is represented in the last two panels of Fig. 1, which shows the poloidal cross sections of the magnetic (third panel) and electrostatic (fourth panel) potentials.

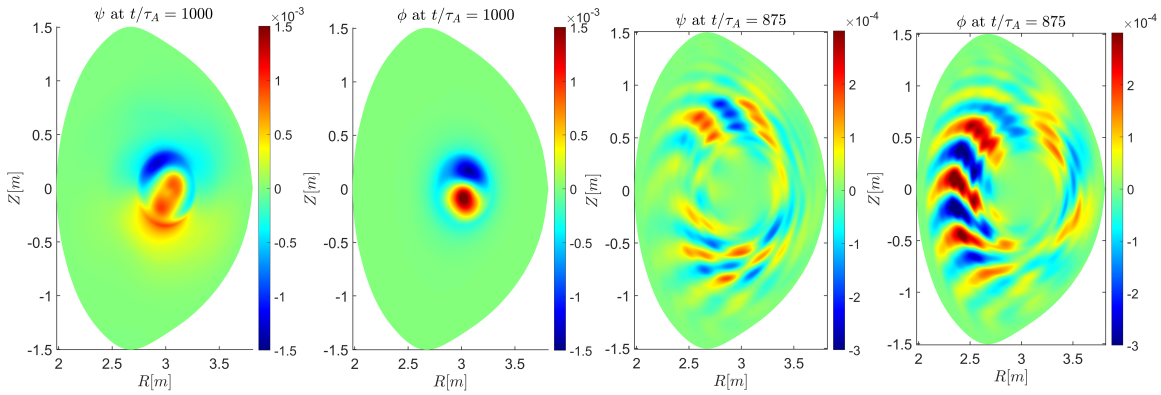

FIG. 1. Snapshots of the poloidal cross sections of the electrostatic and magnetic potentials for the fishbone driven by the trapped population (first two panels) showing the $m = 1$ structure and for the Alfvén mode driven by the passing population (last two panels).

3. OVERVIEW OF THE NEW FULL-ORBIT TOROIDAL ACCELERATED PARTICLE SIMULATOR (TAPAS)

The recently developed Toroidal Accelerated PArticle Simulator (TAPAS) has been significantly upgraded since its first version [5] to include a more realistic description of particles in toroidal fusion devices. It has in particular been extended to a full-orbit version, which is especially important for the physics of highly energetic particles like fusion-born alpha particles. The integration of trajectories is performed in Cartesian coordinates in the 6D phase-space (x, y, z, v_x, v_y, v_z) to facilitate the implementation of the Boris algorithm [6]. In addition, with respect to the initial version of TAPAS, the code integrates now the trajectories in arbitrary magnetic equilibria that can be given to the code from a numerical file containing the magnetic surfaces and the contravariant components of the equilibrium magnetic field. Therefore, magnetic equilibria built using codes like VMEC [7], SIESTA [8, 9] or DESC [10] can be given to TAPAS. The trajectories can be integrated also in the presence of arbitrary 3D electromagnetic fields that can be either analytical or numerical from external codes in generalized coordinates. Since the trajectory integration is done in Cartesian coordinates, TAPAS includes a dedicated module for coordinate transformation from generalized to Cartesian coordinates. The interpolation of the 3D electromagnetic field at the position of the particles is done by means of 3D BSplines. TAPAS has been accelerated on GPUs using a hybrid parallelization based on the MPI-OpenACC paradigm. Lagrange interpolation is employed for 1D or 2D quantities. However, cubic BSplines are used instead for 3D quantities. Moreover, both BSplines and the different diagnostics have been conveniently accelerated on GPU to ensure the optimization of the code. The results of TAPAS are written using the parallel HDF5 library. Special emphasis has been put on the integration of trajectories for particles in the neighbourhood of the last magnetic surface. Also, trajectories that approach the magnetic axis can suffer from numerical instabilities due to possible problems during the magnetic equilibrium reconstruction. For those cases, second-order (resp. third-order) Taylor expansion of the 2D (resp. 3D) magnetic equilibrium is performed.

TAPAS handles the initialization of particles in real space using toroidal coordinates (r, θ, φ). As for the initialization in velocity space, the flexibility of TAPAS allows using different coordinates. The initialization can be done either in 6D, in which case the velocities are initialized using the Cartesian components (v_x, v_y, v_z), or in 5D, in which case the gyro-phase φ_c is randomly sampled from a uniform distribution $\mathcal{U}_{]0,2\pi]}(\varphi_c)$ and the parallel and perpendicular velocities are selected by initializing the particles in (a) $\left(v_\parallel, \mu\right)$, or in (b) (E, Λ), or in (c) (E, λ), or in (d) (E, P_φ). Here, $v_\parallel$ is the velocity parallel to the equilibrium magnetic field, μ is the magnetic moment, E is the kinetic energy, $\lambda = v_\parallel / v$ is the pitch angle, $\Lambda = \mu B_0 / E$ and P_φ is the toroidal canonical momentum. When using initializations (b), (c) or (d), TAPAS applies the required transformations to get the velocity coordinates in terms of $v_\parallel$ and μ. Where in the phase-space particles are initialized depends strongly on the analysis to be performed. In that sense, the initial positions of particles can be specifically selected, for instance using one single energy at a given radial position. This allows total control on the initialization. More realistic initialization can be achieved by sampling a target distribution function. This is done by means of a Metropolis-Hastings algorithm [11], based on Markov Chain Monte Carlo (MCMC) method.

Finally, collisions of particles on a background Maxwellian (composed of both ions and electrons) are introduced in TAPAS using a combination of deterministic and stochastic operators, representing the Coulomb drag and the diffusion, respectively. More details on the new full-orbit TAPAS will be provided in a forthcoming publication [12].

4. TAPAS SIMULATIONS OF FUSION-BORN ALPHA PARTICLES WITH MHD ACTIVITY

4.1. Initialization and prompt losses

Alpha particles are initialized in the inner core of the tokamak, where the main activity occurs, uniformly in radius ($0 < \rho = r/a < 0.25$), poloidal angle ($0 < \theta < 2\pi$) and pitch angle ($-1 < \lambda < 1$), but monoenergetic. Different energies (340 keV, 680 keV, 1 MeV and 1.4 MeV) are chosen to account for the effect of the MHD instabilities depending on the energies of alpha particles. For each of these energies, the number of initialized particles is $N_{\rm part} \sim 10^6$. The perturbation from FAR3d is introduced once the system reaches a statistical steady-state in the sense of prompt losses and redistribution of particles in the tokamak. Indeed, for highly energetic particles, prompt losses (or first orbit losses) can be significant due to the large orbit width of trajectories. Also, particles initialized in the inner region explore regions in the tokamak far from the place where they were initialized. In particular, in our case, the perturbation from FAR3d is introduced after $t/\tau_A = 400$. The left panel of Fig. 2 shows the time evolution of the fraction of lost particles, measured as $f_{\rm lost,\ prompt} = N_{\rm lost}/N_{\rm total}$, for the different energies considered. It is observed that the prompt losses increase with the energy, owing to the dependence of the orbit width on the energy of particles. Also, the steady-state is reached faster for higher energies. The right panel of Fig. 2 represents the fraction of lost particles (prompt losses) at $t/\tau_A = 400$ (when the steady-state is reached) as a function of the initial pitch angle. For relatively low energies, the prompt losses are mainly localized around

$\lambda = -0.4$. Increasing the energy results in a wider region in pitch angle where prompt losses occur, but in general the losses occur mainly for $\lambda < 0.5$. As a result, a strongly anisotropic distribution is formed.

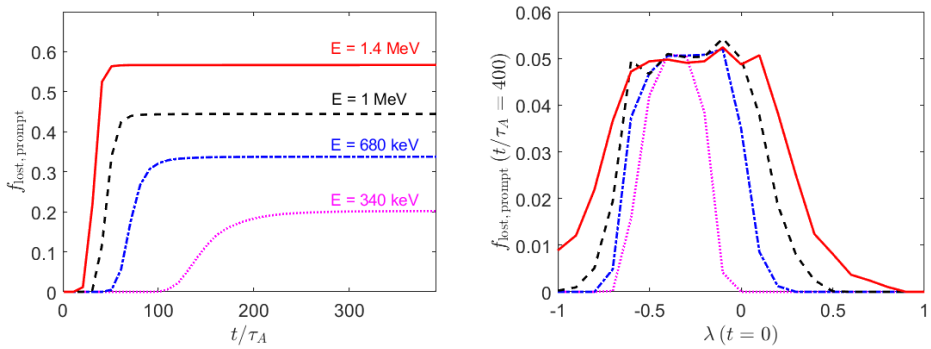

FIG. 2. Fraction of lost particles during the first orbit (prompt losses) as a function of time for different energies (left). For the steady-state regime, before introducing the electromagnetic perturbation, fraction of promptly lost particles as a function of their initial pitch angle and for the different energies considered in the paper (right). The legend for both panels is the same.

4.2. Transport and losses in the presence of fishbones driven by trapped population

Once the statistically steady-state after the prompt losses is reached, we switch on the perturbation from FAR3d characterizing a fishbone excited by trapped Hydrogen. The fraction of lost particles is measured taking as a reference the state of the system at $t/\tau_A = 400$, i.e. we quantify the losses of alpha particles with respect to the number of particles confined in the tokamak after the prompt losses. The quantity of interest is therefore $f_{\text{lost}} = \frac{N_{\text{lost}} - N_{\text{lost, prompt}}}{N_{\text{total}} - N_{\text{lost, prompt}}}$, where N_{lost} is the total number of lost particles as a function of time, which includes also the prompt losses.. Fig. 3 illustrates the impact of the fishbone instability on the confinement of alpha particles. The left (resp. right) panel represents the effect when only the electrostatic (resp. magnetic) component of the instability is introduced in TAPAS. The figure provides the fraction of lost particles for the different energies considered in the paper. It is observed that for relatively low energies, the impact of the electrostatic component is significantly more pronounced than that of the magnetic component. However, when increasing the energy of alpha particles, the impact of the magnetic component becomes comparable to that of the electrostatic component. There is evidence that the fishbone instability that is mainly located in the core region of the tokamak can have deleterious impact on the confinement of alpha particles, leading to up to $25 - 30\%$ of the fraction of particles that is lost for energies of the order of 1 MeV or larger. It is to be reminded that this fraction is calculated with respect to the population that remains confined after the prompt losses. Of course, further analysis is required to estimate the nature of the transport (with respect to the diffusive transport), but this is beyond the scope of the present paper. In the remainder of this subsection, both electrostatic and magnetic components are included to account for the total effect of the instability.

Although the alpha particles are initialized in the inner region, their large orbit widths make them explore larger radial positions. As a result, the position of the alpha particles and their distribution in space (radially and poloidally) depend strongly on their energy and pitch angle. To illustrate this, the top left panel of Fig. 4 shows the final density of all the particles initialized inside the surface $\rho = 0.25$ at the energy $E = 1.4$ MeV (for the sake of clarity only one energy is considered for the top panels of this figure). The color represents the density in a.u. Depending on the pitch angle of the particles, they are mainly localized in the high field side (HFS) for $\lambda < 0$ or in the low field side (LFS) for $\lambda > 0$. This implies that in the presence of a perturbation leading to losses of particles, those with $\lambda < 0$ will be lost in the HFS mid-plane, whereas particles with $\lambda > 0$ will be lost in the LFS mid-plane. This is corroborated by the probability density function (PDF) of the poloidal angle of lost particles for positive and negative pitch angles, as illustrated in the top right panel of Fig. 4. The overall radial impact of the fishbone instability can be observed in the four bottom panels of Fig. 4 for the different energies considered. The curves indicate the number of particles (all pith angles included) as a function of the normalized minor radius. The grey areas represent the profiles once the prompt losses have occurred and the red areas represent the final radial distribution of particles. It is observed that the effect of the fishbone is global, although the mode remains localized in the inner region of the tokamak. This global effect is likely due to the large orbit width of alpha particles. Also, the effect seems to be more pronounced when increasing the energy.

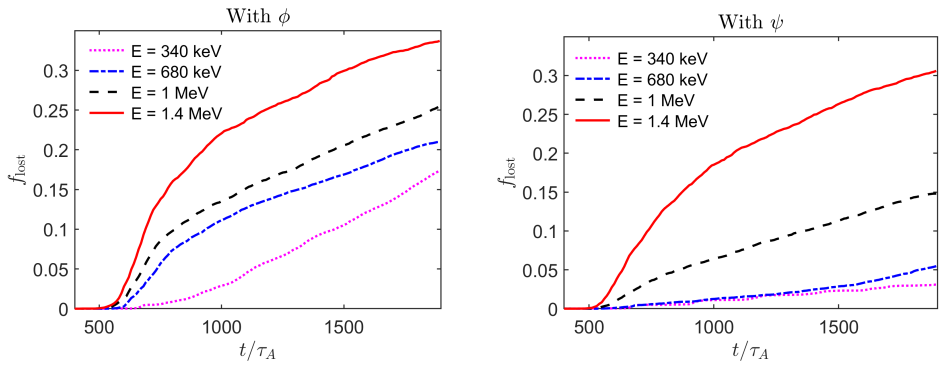

FIG. 3. Fraction of lost particles as a function of time in the presence of the electrostatic (left) or magnetic (right) components of the fishbone mode excited by trapped Hydrogen. The curves are plotted for the different energies of alpha particles considered in the paper.

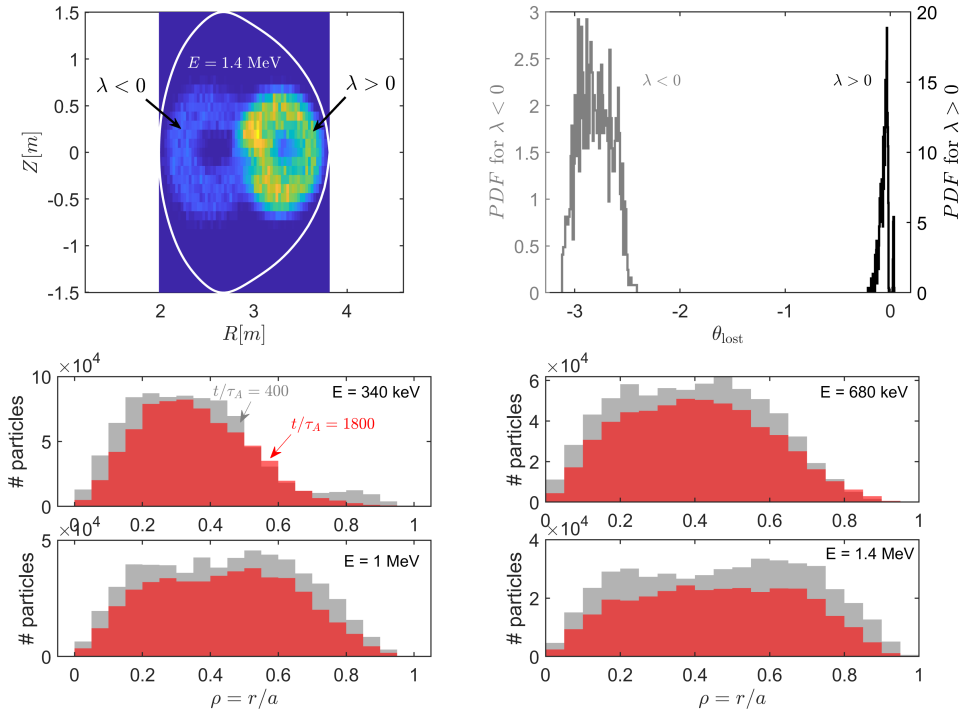

FIG. 4. Poloidal cross section of the final density for alpha particles initialized at $E = 1.4$ MeV (top left). Probability density function (PDF) of the poloidal position at which particles with $E = 1.4$ MeV are lost, highlighting the differences between positive (right axis) and negative (left axis) pitch angles (top right). Radial distribution of particles after the prompt losses (grey areas) and after the fishbone instability (red area) for the different energies considered (bottom panels).

For the considered initialization of particles, analysis of the pitch angle is provided in Fig. 5, where the PDFs of the pitch angle for the confined (left) and lost (right) particles are plotted. The different energies are indicated using the same conveniton as in the previous figures of the paper. It is to be noted that the right panel of the figure represents the PDF of the pitch angle of the particles that are lost only due to the fishbone instability, i.e. we do not consider for the computation of the PDF the particles that are pormptly lost. Several comments can be made based on these figures. The first obvious observation is that the pitch angle has a significant impact on the confinement and losses of the particles. For low energies, particles with positive and negative pitch angles remain roughly equally confined. When the energy is increased, particles with positive pitch angles tend to be better confined than those with negative pitch angles. This is also reflected in the right panel of Fig. 5. Indeed, it is observed that the PDF of lost particles for negative pitch angles increases with the energy. Finally, whereas the PDF of pitch angle for lost particles extends from $\lambda = -1$ up to $\lambda = -0.5$, that of positive pitch angles is mostly localized around $\lambda \approx 0.5$.

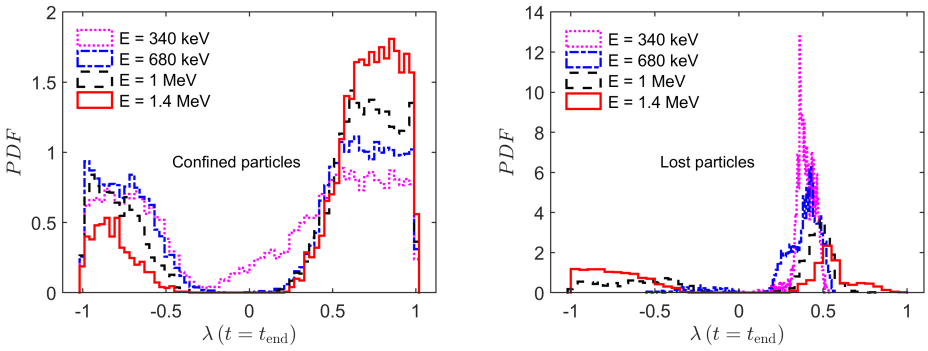

FIG. 5. PDF of the pitch angle for the confined (left) and lost (right) particles for the different energies considered in the paper.

The next analysis concerns the distribution of the energy of confined and lost particles. Let us remind that the particles are monoenergetic in our TAPAS simulations. Fig. 6 represents the PDFs of kinetic energy for the different classes of particles considered in the paper, making the distinction between confined and lost (only due to the perturbation, no prompt losses are considered here, which would introduce a dominant peak in the PDFs of lost particles). Several comments can be made. First, the initially monoenergetic alpha particles remain almost monoenergetic, with variations in the range of $4 - 14\%$. It is interesting to realize that the PDF for confined particles with high energy could be approximated by a Gaussian. This is clearly not the case for relatively low energies. Regarding the PDF for lost particles, they are close to those for confined particles only for intermediate energies $E \approx 1$ MeV. For low energies ($E < 1$ MeV) the PDF are clearly asymmetric, with a more pronounced tail towards low energies.

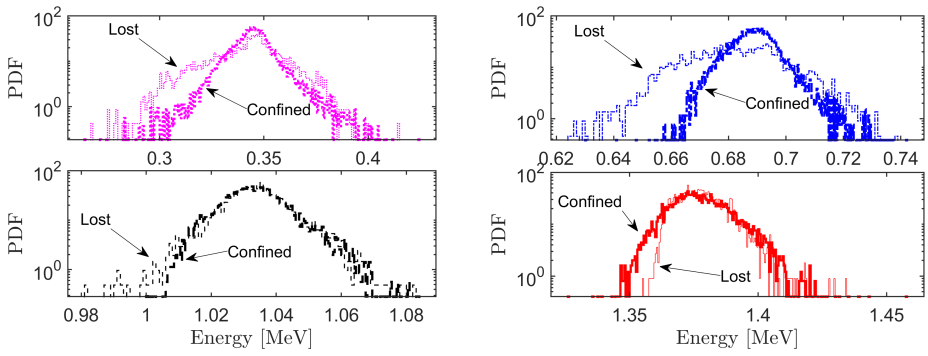

FIG. 6. PDF of the energy for the confined (thick curves)) and lost (thin curves) particles for the different energies considered in the paper.

Finally, after the detailed previous studies with very specific energies for particles initialized inside $\rho = 0.25$, one can conduct more realistic analyses by making use of the Metropolis-Hastings algorithm for the initialization of particles. For this purpose, we initialize $N_{\rm part} \sim 3 \cdot 10^7$ particles sampling the same distribution function as in the

FAR3d simulations, i.e. an equivalent Maxwellian with $T = 1$ MeV, with an initial radial density profile peaking at $\rho = 0$ and decreasing towards 0 for $\rho > 0.5$. We have selected an isotropic distribution, but other types can be envisioned. We have observed that the initially peaked density extends quickly towards larger radial positions due to the large orbit of alpha particles and to the prompt losses, as depicted by the dashed blue line of the left panel of Fig. 7. Once the prompt losses have occurred the fishbone is destabilized and the effect on the density profile is represented by the solid red line. As expected, the impact on the density is over the whole radial positions, more significant in the inner core due to the smaller volume. The effect in phase-space is represented in the right panel of Fig. 7, where we plot in logarithmic scale the difference between the distribution functions before the onset of the fishbone instability and at the end of the simulation. From this analysis no clear resonance is evidenced, which might imply that the losses are not induced by by convective resonant transport. Also, the time trace of the number of lost particles have not revealed any characteristic frequency, implying that the losses are not coherent. Further analysis is required to assess the nature of the alpha particle transport in the presence of fishbones.

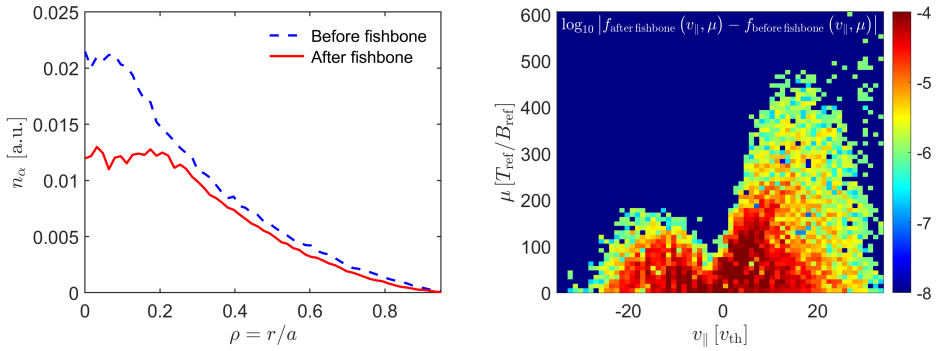

FIG. 7. Density of alpha particles before the onset of the fishbone instability (dashed blue line) and at the end of the simulation (solid red line) (left). Difference between the final distribution function and the one before the onset of the fishbone instability, in logarithmic scale, as a function of the parallel velocity and the magnetic moment for all radial positions (right).

4.3. Transport and losses in the presence of Alfvén Eigenmodes driven by passing population

Similar analysis has been performed for the transport and losses of alpha particles in the presence of the Alfvén modes driven by the passing population. As opposed to the transport and losses induced by the fishbone instability, no significant losses have been observed. The result is summarized in Fig. 8. This is in agreement with experimental observations with the FILD diagnostic.

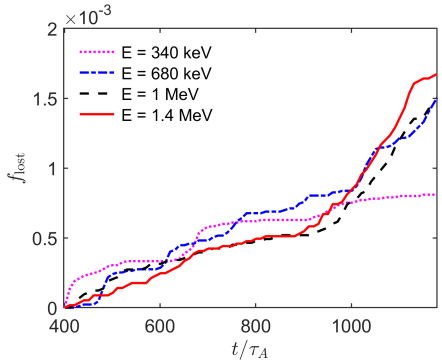

FIG. 8. Fraction of lost particles as a function of time in the presence of the Alfvén activity driven by passing particles including both electrostatic and magnetic components.

5. CONCLUSIONS

The impact of MHD instabilities driven by energetic particles on the transport and losses of fusion-born alpha particles has been analysed in the framework of the last DT experimental campaign at JET. In particular, the discharge 99896 has been modelled using a combination of gyro-fluid simulations performed with FAR3d code and full-orbit trajectory integration using TAPAS code. Special emphasis has been put on the impact of instabilities driven by trapped particles (fishbones) and passing particles (TAE). Significant losses in the presence of fishbone activity has been observed, mainly due to the losses of co- and counter-passing alpha particles near the equatorial plane at the HFS ($\lambda < 0$) and at the LFS ($\lambda > 0$). Analysis of the distribution function in velocity space does not reveal any signficant resonance, suggesting that the losses might not be due to any convective resonant transport. Furthermore, the losses in the presence of higher frequency Alfvén modes have been observed to be negligible, in agreement with experimental observations. Further analyses need to be performed to take into account the effect of collisions. Moreover, in-depth studies of the nature of the transport of alpha particles together with reduced models must be conducted.

ACKNOWLEDGEMENTS

This work has been carried out within the framework of the EUROfusion Consortium, funded by the European Union via the Euratom Research and Training Programme (Grant Agreement No 101052200 — EUROfusion). Views and opinions expressed are however those of the author(s) only and do not necessarily reflect those of the European Union or the European Commission. Neither the European Union nor the European Commission can be held responsible for them. This work has received financial support from the AIM4EP project (ANR-21-CE30-0018), funded by the French National Research Agency (ANR), from the Comunidad de Madrid under the project 2019-T1/AMB-13648, and from the Oak Ridge National Laboratory, managed by UT-Battelle, LLC, for the US Department of Energy under Contract No. DE-AC05-00OR22725. TAPAS simulations were performed on HPC resources of IDRIS under the allocations 2021-A0100512455, 2022-AD010512455R1 and 2023-A0140514165 made by GENCI. TAPAS development, optimization and deployment on GPU accelerator were done within the framework of an advanced support program funded by IDRIS and GENCI.

REFERENCES

[1] HEIDBRINK W. W. and SADLER G. J. *Nuclear Fusion*, 34(4):535, 1994.

[2] SHARAPOV S. E. et al. *Nuclear Fusion*, 40(7):1363, 2000.

[3] GARCIA J. et al. *Science Advances*, Submitted.

[4] SPONG D. A. et al. *Nuclear Fusion*, 61(11):116061, 2021.

[5] ZARZOSO D. et al. *Plasma Physics and Controlled Fusion*, 64(4):044003, 2022.

[6] BORIS J. P. et al. In *Proc. Fourth Conf. Num. Sim. Plasmas*, pages 3–67, 1970.

[7] HIRSHMAN S. P. and Whitson J. C. *The Physics of fluids*, 26(12):3553–3568, 1983.

[8] HIRSHMAN S. P. et al. *Physics of Plasmas*, 18(6), 2011.

[9] PERAZA-RODRIGUEZ H. et al. *Physics of Plasmas*, 24(8), 2017.

[10] PANICI D. et al. *Journal of Plasma Physics*, 89(3):955890303, 2023.

[11] HASTINGS W. K. 1970.

[12] BETAR H. et al. in preparation.